

Single-Molecule Orientation Determination With Polarized Illumination: Modeling and Microscope Design Comparison

TALON CHANDLER,^{1,*} SHALIN MEHTA,² RUDOLF OLDENBOURG,^{2, 3}
AND PATRICK J. LA RIVIÈRE¹

¹*University of Chicago, Department of Radiology, Chicago, IL, USA.*

²*Marine Biological Laboratory, Bell Center for Regenerative Medicine, Woods Hole, MA, USA.*

³*Brown University, Department of Physics, Providence, RI, USA.*

*talonchandler@talonchandler.com

Abstract: TODO

OCIS codes: (180.0180) Microscopy; (260.5430) Polarization; (110.0110) Imaging systems; (180.2520) Fluorescence microscopy; (180.6900) Three-dimensional microscopy.

References and links

1. J. T. Fourkas, “Rapid determination of the three-dimensional orientation of single molecules,” *Opt. Lett.* **26**, 211–213 (2001).
2. R. Oldenbourg and G. Mei, “New polarized light microscope with precision universal compensator,” *Journal of Microscopy* **180**, 140–147 (1995).
3. Y. Wu, P. Wawrzusin, J. Senseney, R. S. Fischer, R. Christensen, A. Santella, A. G. York, P. W. Winter, C. M. Waterman, Z. Bao, D. A. Colon-Ramos, M. McAuliffe, and H. Shroff, “Spatially isotropic four-dimensional imaging with dual-view plane illumination microscopy,” *Nat Biotech* **31**, 1032–1038 (2013). Research.
4. Y. Wu, P. Chandris, P. W. Winter, E. Y. Kim, V. Jaumouillé, A. Kumar, M. Guo, J. M. Leung, C. Smith, I. Rey-Suarez, H. Liu, C. M. Waterman, K. S. Ramamurthi, P. J. La Riviere, and H. Shroff, “Simultaneous multiview capture and fusion improves spatial resolution in wide-field and light-sheet microscopy,” *Optica* **3**, 897–910 (2016). 27761486[pmid].
5. S. M. Kay, *Fundamentals of statistical signal processing* (Prentice Hall PTR, 1993).
6. A. Agrawal, S. Quirin, G. Grover, and R. Piestun, “Limits of 3d dipole localization and orientation estimation for single-molecule imaging: towards green’s tensor engineering,” *Opt. Express* **20**, 26667–26680 (2012).
7. T. W. Anderson, T. W. Anderson, T. W. Anderson, T. W. Anderson, and E.-U. Mathématicien, *An introduction to multivariate statistical analysis*, vol. 2 (Wiley New York, 1958).

1. Introduction

TODO:

- General paragraph about the dipole orientation imaging.
- Current state of the art: scanning, detection polarization modulation, geometries
- We propose single-molecule orientation determination with polarized illumination. Compare with others. Highly parallel imaging for live cells.
- Section by section summary.

2. Methods

In this section we will develop a method to compare polarized illumination microscope designs. In sections 2.1–2.4 we develop the forward model for single-frame microscopes with a fixed illumination and detection orientation. In section 2.5 we list a variety of ways that single-frame microscopes can be combined to create experimentally realizable multi-frame microscopes. Finally, in section 2.6 we develop metrics that we will use to compare multi-frame microscopes.

2.1. Excitation Efficiency

Consider polarized Köhler illumination incident on a single fluorophore at the focal point with the optical axis aligned along the $\hat{\mathbf{z}}$ axis. In this section we will calculate the *excitation efficiency* in this geometry—the fraction of the incident power that excites the fluorophore.

We start with the unit electric field transmitted by the polarizer,

$$\hat{\mathbf{E}}_{\text{exc}} = \cos \phi_{\text{exc}} \hat{\mathbf{x}} + \sin \phi_{\text{exc}} \hat{\mathbf{y}}, \quad (1)$$

where ϕ_{exc} is the angle between the transmission axis of the excitation polarizer and the $\hat{\mathbf{x}}$ axis. Next, we model the action of the illumination lens by multiplying the electric field vector by a position dependent rotation matrix,

$$\mathbf{R}(\hat{\mathbf{r}}) = \begin{bmatrix} \cos \theta \cos^2 \phi + \sin^2 \phi & (\cos \theta - 1) \sin \phi \cos \phi & -\sin \theta \cos \phi \\ (\cos \theta - 1) \sin \phi \cos \phi & \cos \theta \sin^2 \phi + \cos^2 \phi & -\sin \theta \sin \phi \\ \sin \theta \cos \phi & \sin \theta \sin \phi & \cos \theta \end{bmatrix} \quad (2)$$

where

$$\hat{\mathbf{r}} = \sin \theta \cos \phi \hat{\mathbf{x}} + \sin \theta \sin \phi \hat{\mathbf{y}} + \cos \theta \hat{\mathbf{z}} \quad (3)$$

is a unit vector that points from the origin to the point where the incident electric field intersects the Gaussian sphere of the condenser lens. Next, we find the power that excites the fluorophore by taking the dot product of the rotated incident field $\mathbf{R}(\hat{\mathbf{r}})\hat{\mathbf{E}}_{\text{exc}}$ and the excitation dipole moment

$$\hat{\mu}_{\text{exc}} = \sin \Theta \cos \Phi \hat{\mathbf{x}} + \sin \Theta \sin \Phi \hat{\mathbf{y}} + \cos \Theta \hat{\mathbf{z}} \quad (4)$$

then taking its modulus squared. If the incident fields are spatially incoherent then we can find the total power that excites the fluorophore by integrating over the illuminated region of the Gaussian sphere Ω where

$$\Omega = \{(\phi, \theta) \mid \phi \in (0, 2\pi], \theta \in [0, \alpha]\} \quad (5)$$

$$\alpha = \arcsin\left(\frac{\text{NA}}{n}\right). \quad (6)$$

Finally, we find the fraction of the incident power that excites the fluorophore by dividing the total excitation power by the total incident power. The complete expression for the excitation efficiency in vector notation is

$$\eta_{\text{exc}} = \frac{\int_{\Omega} d\hat{\mathbf{r}} |\hat{\mu}_{\text{exc}} \cdot \mathbf{R}(\hat{\mathbf{r}})\hat{\mathbf{E}}_{\text{exc}}|^2}{\int_{\Omega} d\hat{\mathbf{r}}}. \quad (7)$$

We can substitute equations 1–6 into equation 7 and simplify to express the excitation efficiency in scalar notation as

$$\eta_{\text{exc}} = D \{ A + B \sin^2 \Theta + C \sin^2 \Theta \cos [2(\Phi - \phi_{\text{exc}})] \} \quad (8)$$

where

$$A = \frac{1}{4} - \frac{3}{8} \cos \alpha + \frac{1}{8} \cos^3 \alpha \quad (9a)$$

$$B = \frac{3}{16} \cos \alpha - \frac{3}{16} \cos^3 \alpha \quad (9b)$$

$$C = \frac{7}{32} - \frac{3}{32} \cos \alpha - \frac{3}{32} \cos^2 \alpha - \frac{1}{32} \cos^3 \alpha \quad (9c)$$

$$D = \frac{4}{3(1 - \cos \alpha)}. \quad (9d)$$

At the beginning of this section we assumed that the fluorophore was located at the focal point of the condenser. If the condenser is aplanatic then we can relax this assumption and the above expressions are valid for fluorophores anywhere in the focal plane.

We also assumed that we are using incoherent Köhler illumination. If we illuminate the back aperture with a weakly focused laser beam and scan the laser beam slowly compared to the coherence time of the laser, the fluorophore will be excited as if it were excited by a single plane wave. Therefore, we can find the excitation efficiency of weakly focused scanned laser illumination by taking the limit of equation 8 as $\alpha \rightarrow 0$ which gives

$$\eta_{\text{exc}} = \sin^2 \Theta \cos^2(\Phi - \phi_{\text{exc}}).$$

2.2. Detection Efficiency

Fourkas calculated the detection efficiency of a single fluorophore when an objective with a polarizer is aligned along the $\hat{\mathbf{z}}$ axis [1]. We use his expressions to calculate the detection efficiency without a polarizer as

$$\eta_{\text{det}} = 2(A + B \sin^2 \Theta). \quad (10)$$

Note that the detection efficiency only depends on Θ , not Φ , because there is no detection polarizer. Also note that A and B in equation 9 are a factor of $\frac{3}{2}$ larger than the expressions given by Fourkas. We found that Fourkas' expressions were incorrectly normalized, and the extra factor of $\frac{3}{2}$ corrects the error.

2.3. Oblique Illumination and Detection

In sections 2.1 and 2.2 we assumed that both the illumination and detection objectives had $\hat{\mathbf{z}}$ aligned optical axes. To extend the forward model to oblique optical axes, we express the dipole orientation in rotated coordinates using the following expressions

$$\theta' = \arccos(\sin \psi \cos \Phi \sin \theta + \cos \psi \cos \theta) \quad (11)$$

$$\Phi' = \begin{cases} \arccos\left(\frac{\cos \psi \cos \Phi \sin \theta - \sin \psi \cos \theta}{\sqrt{1 - (\sin \psi \cos \Phi \sin \theta + \cos \psi \cos \theta)^2}}\right) & 0 \leq \Phi < \pi \\ -\arccos\left(\frac{\cos \psi \cos \Phi \sin \theta - \sin \psi \cos \theta}{\sqrt{1 - (\sin \psi \cos \Phi \sin \theta + \cos \psi \cos \theta)^2}}\right) & -\pi \leq \Phi < 0 \end{cases} \quad (12)$$

where ψ is the angle that the optical axis makes with the $\hat{\mathbf{z}}$ axis in the $\hat{\mathbf{x}}$ direction.

2.4. Single-Frame Microscopes

The detected intensity is the product of the excitation efficiency, the detection efficiency, and the total intensity emitted by the fluorophore if the excitation and detection efficiency were 1

$$I = I_{\text{tot}} \eta_{\text{exc}} \eta_{\text{det}}. \quad (13)$$

Equation 13 is the forward model for a *single-frame microscope*. Figure 1 shows three representative examples of single frame microscopes.

The intensity measured by a single-frame microscope does not give us enough information to reconstruct the 3D orientation of a single fluorophore. Next, we will consider combining several single-frame microscopes to create *multi-frame microscopes*.

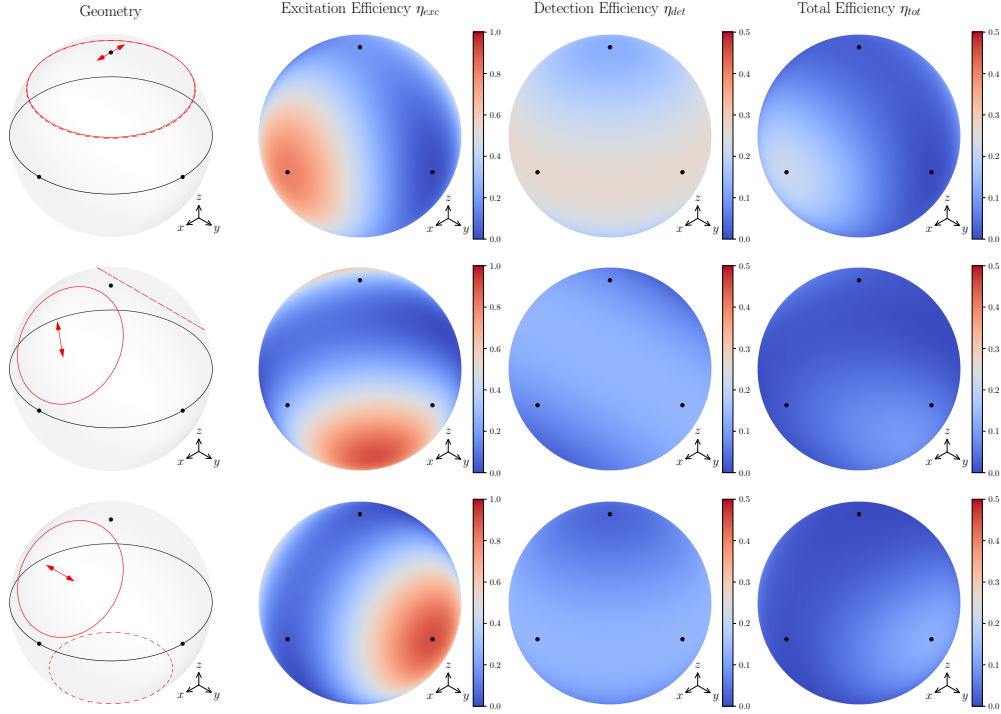


Fig. 1. Representative examples of single-frame microscopes.

Columns left to right: 1) schematics of single-frame microscopes where the solid line encloses the illumination solid angle, the dashed line encloses the detection solid angle, and the arrow indicates the transmission axis of the illumination polarizer; 2) the excitation efficiency, see equation 8; 3) the detection efficiency, see equation 10; (4) the total efficiency, the product of the detection and excitation efficiencies.

Rows top to bottom: 1) epi-illumination ($NA = 1.1$) with x -polarized light and epi-detection ($NA = 1.1$); 2) orthogonal illumination ($NA = 0.8$) and detection ($NA = 0.8$); 3) oblique illumination ($NA = 0.8$) and detection ($NA = 0.8$).

2.5. Multi-Frame Microscopes

One way to collect multiple frames is to add a universal compensator to the illumination arm and rapidly select the incident polarization by changing ϕ_{exc} [2]. All of the multi-frame microscopes we will consider in this paper use a universal compensator with four polarization settings separated by 45° .

We also consider designs that use extra detection and illumination arms. Wu et al. have implemented a microscope that uses orthogonal objectives that can act as both illumination and detection arms [3]. Wu et al. has also added a third view to their microscopes to further improve resolution [4]. We will explore the possibility of using these geometries for orientation determination of fluorophores.

2.6. Evaluation Metrics

Our goal is to evaluate the ability of a microscope design to estimate the parameters Θ and Φ from intensity data.

For each microscope design and fluorophore orientation we calculate the Fisher information matrix. If the intensity is Poisson distributed the Fisher information matrix is given by

$$\mathbf{F} = \sum_{k=1}^N \frac{1}{I_k} \begin{bmatrix} \frac{\partial I_k}{\partial \Theta} \frac{\partial I_k}{\partial \Theta} & \frac{\partial I_k}{\partial \Theta} \frac{\partial I_k}{\partial \Phi} \\ \frac{\partial I_k}{\partial \Phi} \frac{\partial I_k}{\partial \Theta} & \frac{\partial I_k}{\partial \Phi} \frac{\partial I_k}{\partial \Phi} \end{bmatrix} \quad (14)$$

where I_k is the forward model for the k th frame of an N frame microscope.

A common way to evaluate the ability to estimate the parameters Θ and Φ from the data is to calculate the Cramer-Rao lower bound (CRLB) for each parameter [5]. The CRLBs are given by the diagonal elements of the inverse of the Fisher information matrix and they give the minimum variance of unbiased estimators for each parameter. Some authors use the product of the CRLBs multiplied by the Jacobian determinant to find the area of uncertainty in parameter space [6].

CRLBs and the associated area of uncertainty are parametrization dependent—if we choose a different coordinate system then the values will change significantly. We would like to compare microscope designs without choosing a parametrization.

Instead of taking the product of the CRLBs, we use

$$\sigma_\Omega = \sin \Theta \sqrt{\det\{\mathbf{F}^{-1}\}} \quad (15)$$

as our evaluation metric. We take the determinant of the inverse Fisher information matrix—a parametrization independent value often called the *generalized variance* [7]—take the square root, then multiply by the Jacobian determinant, $\sin \Theta$. We call σ_Ω the *solid-angle uncertainty* because it has units of steradians and is a measure of the uncertainty of the orientation parameters.

We calculated σ_Ω on 100,000 approximately equally spaced points on the unit sphere for each microscope design. A desirable microscope design will have a small solid-angle uncertainty that is uniform for all fluorophore orientations. To summarize and compare microscope designs we use the mean and standard deviation of the solid-angle uncertainty at the sample points. Because the solid-angle uncertainty admits unbounded values, we ignore the highest percentile of the sample points and take the mean and standard deviation of the 0-99th percentile.

3. Results

3.1. One-Arm Designs

- Figure 2 shows the results when we used a single objective to illuminate and detect.
- We swept through the illumination and detection NA while keeping the incident power (I_{tot}) constant and found that the lowest mean and standard deviation of the solid-angle uncertainty occurs with a small illumination NA and a large detection NA.

- A small illumination NA maximizes the “contrast” in the excitation efficiency, while a large detection NA maximizes the “contrast” in the detection efficiency.

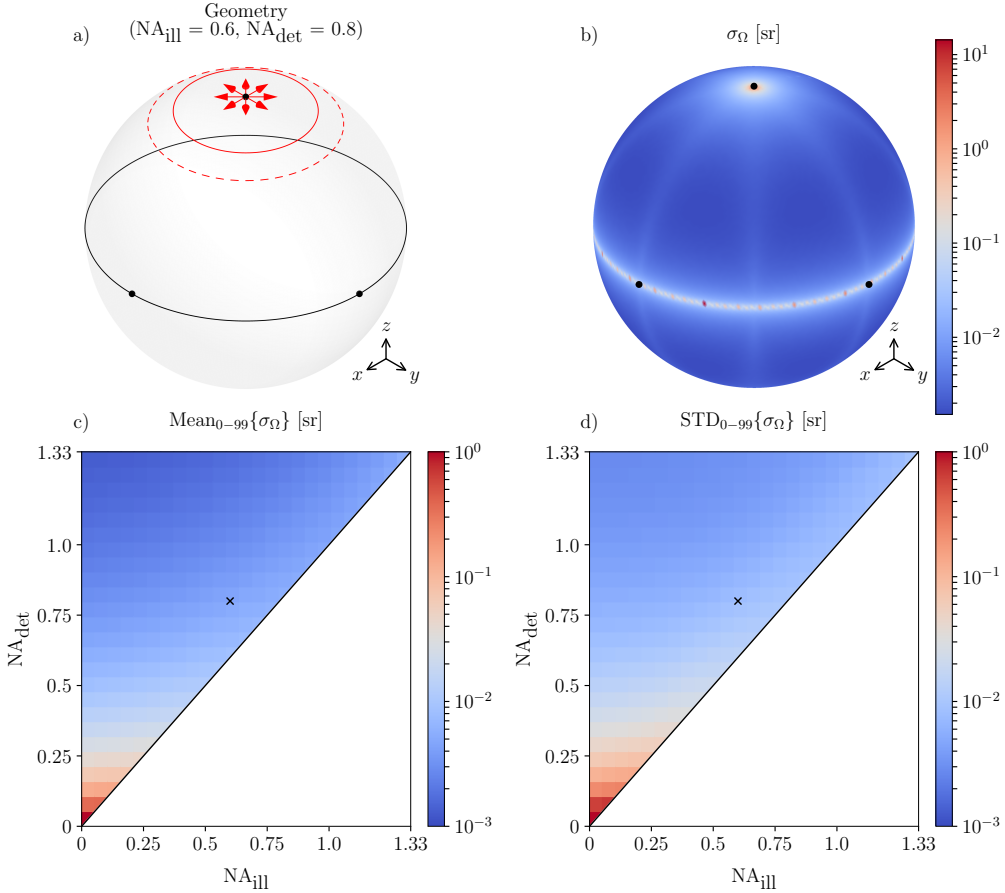


Fig. 2. Epi-illumination microscope with varying NA and underfilling of the back aperture. a) Schematic of a single-arm four-frame epi-illumination microscope. b) Solid angle uncertainty for the microscope in a) when $I_{\text{tot}} = 1000$ photons. c) Mean of the solid-angle uncertainty as a function of illumination and detection NA. d) Standard deviation of solid-angle uncertainty as a function of illumination and detection NA. The microscope in a) and b) is indicated by a cross in c) and d).

3.2. Two-Arm Designs

- Figure 3 shows the results when we used a symmetric widefield design. Both objectives serve as an illumination and detection NA.
- We swept through the NA and the angle between the objectives while considering steric constraints and while keeping the incident power constant. We found that the lowest mean and standard deviation of the solid-angle uncertainty occurs with orthogonal arms with the highest possible NA.
- Figure 4 shows the results when we used a symmetric widefield design and varied the illumination and detection NA.

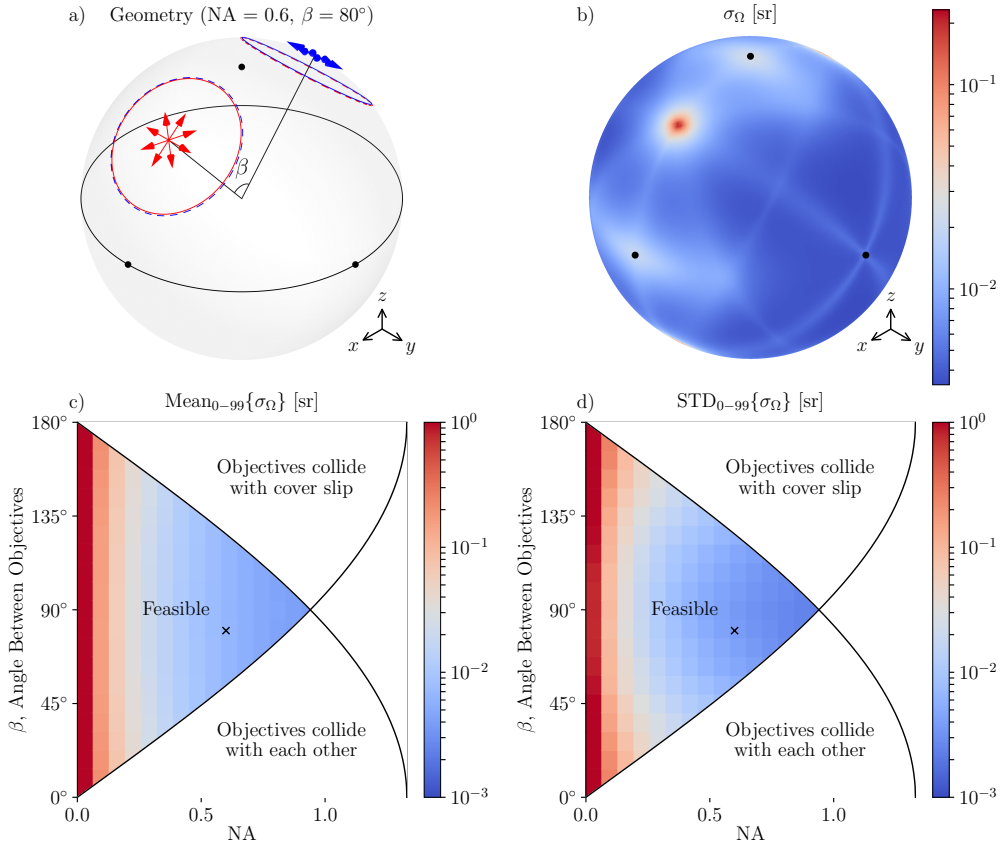


Fig. 3. Symmetric widefield designs with varying NA and angle between objectives. See the Fig. 2 caption for an explanation of a-d).

- Similar to section 3.1, we found that the best microscopes occur with a large detection NA and a small illumination NA (like light sheet illumination).
- Figure 5 shows the results when we considered asymmetric light-sheet designs. We kept the two arms orthogonal and used light-sheet illumination. We swept the NA asymmetry and the dose asymmetry and found that the best results occur for symmetric designs.
- There is a tradeoff between solid-angle uncertainty mean and variance. You can slightly reduce the mean or variance by using an asymmetric design, but you pay for it. Reducing the mean increases the variance and vice-versa.
- The best dual arm microscope design is a symmetric light-sheet illumination microscope with the largest possible detection NA.

3.3. Three-Arm Designs

- Figure 6 shows the results when we considered symmetric light-sheet designs with a lower detection arm. We swept through the NA of the upper arms and NA of the lower arm.
- The results show that the best designs have the largest possible detection upper and lower NA.

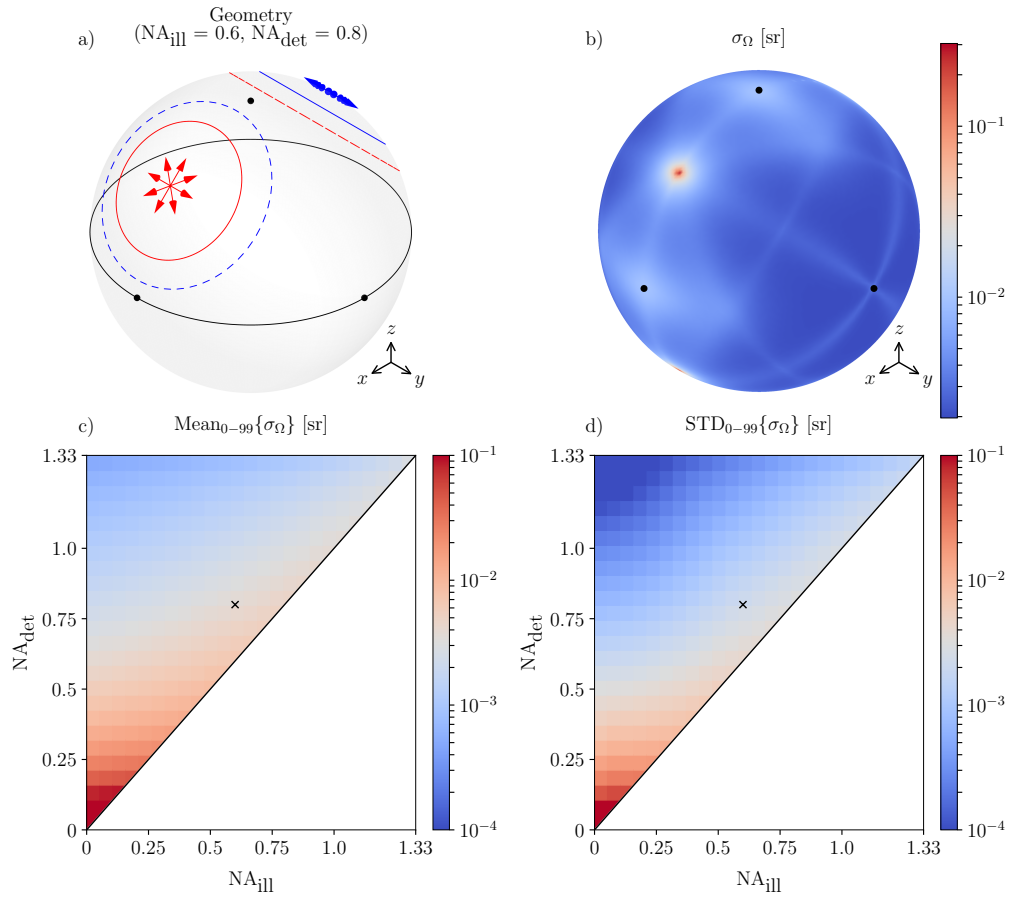


Fig. 4. Symmetric widefield designs with varying NA and underfilling of the back aperture. See the caption for Fig. 2 for an explanation of a)-d).

- Note to Patrick: I used the same efficiencies for the upper and lower arms. I'm still thinking/unsure about the factor of ~1/9 due to rolling shutter on the lower objective. If we do end up using this factor it will weight the importance of a large NA on the upper objectives.

4. Discussion

TODO

5. Conclusion

TODO

Funding

TODO

Acknowledgments

TODO

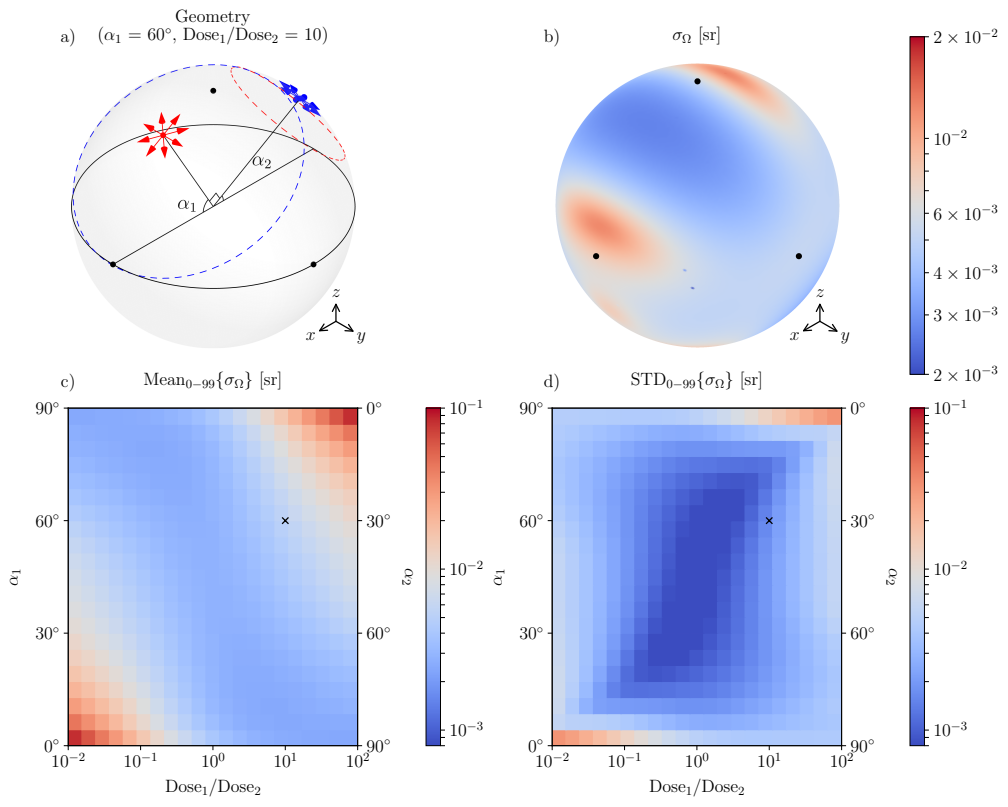


Fig. 5. Asymmetric light-sheet illumination designs with varying NA and dose asymmetry.
 See the Fig. 2 caption for an explanation of a)-d).

Disclosures

TODO

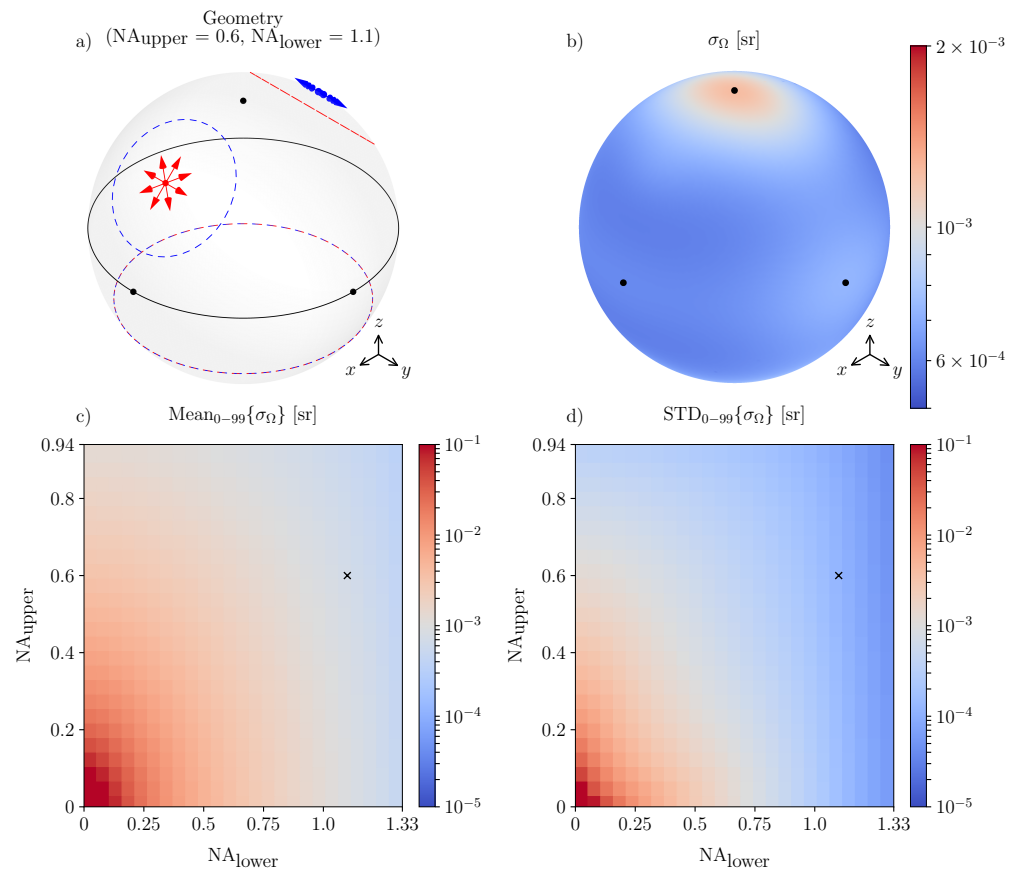


Fig. 6. Symmetric light-sheet illumination with lower detection arm and varying upper and lower NA. See the Fig. 2 caption for an explanation of a)-d).